Impact of Wettability Alteration on the Front Instability of Immiscible Displacement in Porous Media

Hosseinzadehsadati, S.; Eftekhari, A.A.; M. Nick, H.

Published in:
Water Resources Research

Link to article, DOI:
10.1029/2022WR032256

Publication date:
2022

Document Version
Publisher's PDF, also known as Version of record

AGU ADVANCING EARTH AND SPACE SCIENCE

Water Resources Research

RESEARCH ARTICLE
10.1029/2022WR032256

Special Section:
Modeling, simulation, and big data techniques in subsurface fluid flow and transport

Impact of Wettability Alteration on the Front Instability of Immiscible Displacement in Porous Media

S. Hosseinzadehsadati[1], A. A. Eftekhari[1], and H. M. Nick[1]

[1]Danish Offshore Technology Centre, Technical University of Denmark, Copenhagen, Denmark

Key Points:

- Fingering evolution due to the dynamic wettability change is analyzed
- The importance of changing the relative permeability parameters is studied for the onset of instability
- A significant shifting of wettability toward the wetting phase leads to longer fingers and early water breakthrough

Supporting Information:

Supporting Information may be found in the online version of this article.

Correspondence to:

S. Hosseinzadehsadati,
behzadh@dtu.dk

Citation:

Hosseinzadehsadati, S., Eftekhari, A. A., & Nick, H. M. (2022). Impact of wettability alteration on the front instability of immiscible displacement in porous media. *Water Resources Research*, *58*, e2022WR032256. https://doi.org/10.1029/2022WR032256

Received 28 FEB 2022
Accepted 22 NOV 2022

Abstract Wettability alteration that occurs as a result of changing the brine composition or using chemicals that lower the interfacial tension can significantly alter the mobility of nonaqueous liquid (NAPL)/water phases. Here, we show that including dynamic wettability alternation (moving from non-water-wet to water-wet) or interpolating between two sets of relative permeability curves may create an unstable displacement of the residence-fluid by the injected fluid. The instability occurs due to not only the viscosity ratio but also the new shape of relative permeability curves and their end-point values. We perform a full factorial design on Corey relative permeability parameters to determine the most destabilizing factors when the viscosity ratio is one. The observations indicate that instability proliferates when the end-point relative permeability to the NAPL phase of modified salinity brine increases, and their corresponding exponents decrease compared with high salinity brine (seawater or formation water). Besides, numerical simulations of such a displacement demonstrate that modified salinity water (MSW)'s breakthrough is accelerated by wettability change toward water-wet compared with a non-fingering analytical solution. This may result in a delayed mobilization of the NAPL phase in porous media. We also discuss the role of capillary pressure, heterogeneity, and secondary and tertiary injection of MSW in stabilizing the shock front.

1. Introduction

Fingering instability may take place at the interface between two fluids when two immiscible fluids compete in a porous medium. When a less viscous fluid is injected, displacing a more viscous fluid, the created instability is called viscous fingering (Saffman & Taylor, 1958). Many experimental and numerical studies have addressed the viscous fingering instability of two-phase immiscible flow in porous media (Chuoke et al., 1959; Glass et al., 1989; Nicolaides et al., 2015; Peters & Flock, 1981; Riaz & Tchelepi, 2006b; Sarma, 1986). The source of instability is widely linked to viscosity variation between fluids or within components of a single fluid in porous media (Homsy, 1987). In the heterogeneous porous medium, different resistivity paths also cause variations in the fluid velocities which is called channeling (Birkholzer & Tsang, 1997). Nevertheless, viscous fingering and channeling are not classified into the same group. The former occurs as a result of unstable viscously driven flow while the latter is caused by the heterogeneity of porous media (Farthing et al., 2012). Commonly, the mobility ratio (M) is used to evaluate the front instability. This ratio is defined as the mobility (λ) of the displacing fluid to the mobility of the displaced fluid to consider both viscosity and effective permeability impacts ($M = \lambda_{\text{displacing}}/\lambda_{\text{displaced}} = (K/\mu)_{\text{displacing}}/(K/\mu)_{\text{displaced}}$).

The numerical analyses of front instability of immiscible displacement mainly focus on viscous instabilities between two immiscible fluids that are dependent on the viscosity ratio (An et al., 2020; Bakharev et al., 2020; Chuoke et al., 1959; Gorell & Homsy, 1983; Peters & Flock, 1981; Sorbie et al., 2020; Yuan et al., 2021). Some studies also emphasize the impact of physical diffusion and dispersion (Christie & Bond, 1987), heterogeneity of the system (Farthing et al., 2012; Luo et al., 2018), and capillary pressure (Berg & Ott, 2012; Chen et al., 2017; Ott & Berg, 2013) on the front instability. Tripathi and Mohanty (2008) report that wettability alteration at the shock front of an injected fluid may also lead to the front fingering by mobilizing nonaqueous phase liquid (nonaqueous liquid [NAPL]) at its residual saturation that causes an unstable mobility front when NAPL's viscosity is higher than that of water. For example, rock wettability and interfacial tension are commonly altered by adding surfactants and/or polymer, altering salinity, or increasing the temperature into/of the aqueous phase (Bear, 1972; Dullien, 1979; Lake, 1989; Mahani et al., 2017) to mobilize NAPLs for the purpose of contaminated groundwater remediation, and enhanced oil recovery (LaForce & Johns, 2005; Schmid et al., 2011). However, the mobility ratio at the shock front is not only a function of viscosity but also the new saturation and relative permeability curve. Since the relative permeability of injection water differs from in situ water, the mobility ratio may increase across the shock front resulting in a poor sweep efficiency, even for the same viscosity ratio

of water and NAPL, which is the goal of this study. Al-Ibadi et al. (2021) observe that pulse-like behavior also appears in coarse grid simulations of wettability alteration mechanism because of temporarily increasing NAPL flux relative to water by interpolation between two sets of relative permeability curves. They conclude that the instability is caused by the numerical technique and can be resolved by using fine grid blocks. Here, however, we investigate the shock front instability that occurs as the consequence of the intrinsic behavior of the system and mobility ratio contrast observed in the experiments (Glass et al., 1989), not because of the numerical technique. Although the experimental observation shows the importance of rock wettability for the onset of instability, little attention has been paid to systematically addressing the influence of the dynamic change of wettability on the flow instability of the system.

In this study, we describe the physical mechanisms of fingering evolution due to the dynamic wettability change in the absence of viscosity variation or density contrast in the context of modified salinity water (MSW) flooding (Khishvand et al., 2017). MSW injection is previously used for enhancing the performance of the surfactant-assisted NAPL remediation and the enhanced oil recovery (Karadimitriou et al., 2019). In our analysis for MSW flooding, we investigate the total mobility ratio across the shock front between MSW and high salinity water such as formation water (FW) or seawater (SW). The condition for the onset of instability is studied by changing the relative permeability parameters due to wettability alteration. The full factorial design is used for identifying the most affecting factors based on the Corey correlation. Further, the capillary pressure is included to provide more insight into the impact of capillarity on the growth rate of instability. Lastly, we discuss whether or not the induced front instability has an adverse impact on the performance of MSW flooding as an improved recovery/removal method.

2. Methods

Eclipse 100 simulator (Schlumberger simulator) is used in this study to examine perturbation growth between injected water and reservoir fluids due to wettability alteration. In the following sections, we briefly describe the effect of wettability alteration as well as fractional flow theory for 1D immiscible displacement and simulation assumptions.

2.1. Wettability Alteration Modeling

Wettability is a pore-scale property that influences the relative mobility, location and spatial distribution of fluid phases in porous media (Anderson, 1987; Kassa et al., 2021). The wettability alteration caused by physicochemical interactions between the rock, and the injected and formation fluids is assumed to directly change the shape of relative permeability and capillary pressure curves (Hosseinzadehsadati et al., 2022a, 2022b; Lake, 1989). Corey's equation can be used to describe the relative permeability function (Brooks & Corey, 1966),

$$S_w^* = \frac{S_w - S_{\mathrm{wi}}}{1 - S_{\mathrm{wi}} - S_{\mathrm{nr}}} \tag{1}$$

$$k_{\mathrm{rw}} = k_{\mathrm{rw,max}}(S_w^*)^{n_w} \tag{2}$$

$$k_{\mathrm{rn}} = k_{\mathrm{rn,max}}(1 - S_w^*)^{n_n} \tag{3}$$

where S_w is water saturation, S_{wi} is irreducible water saturation, S_{nr} is residual NAPL phase saturation, and n_w and n_n are Corey's exponents for water and NAPL phase, respectively. Here, we assume that all of Corey's parameters are salinity-dependent.

Simple interpolations are used between SW or FW and MSW relative permeability and capillary pressure curves (usually FW for secondary and SW for tertiary displacement mode) to include the effect of modified salinity and its mixing with formation fluid (Jerauld et al., 2008),

$$K_{\mathrm{rw}} = \theta k_{\mathrm{rw}}^{\mathrm{MSW}} + (1-\theta)k_{\mathrm{rw}}^{\mathrm{FW/SW}} \tag{4}$$

$$K_{\mathrm{rn}} = \theta k_{\mathrm{rn}}^{\mathrm{MSW}} + (1-\theta)k_{\mathrm{rn}}^{\mathrm{FW/SW}} \tag{5}$$

$$P_{\mathrm{cnw}} = \theta P_{\mathrm{cnw}}^{\mathrm{MSW}} + (1-\theta)P_{\mathrm{cnw}}^{\mathrm{FW/SW}} \tag{6}$$

where θ is the scaled salinity weighting factor between high and modified salinity curves, P_{cnw} is capillary pressure, K_{rw} is effective water relative permeability, K_{rn} is effective NAPL phase relative permeability. FW/SW and MSW superscripts indicate FW or SW and MSW, respectively.

2.2. 1D Transport Model

Neglecting gravity and capillary pressure, the two-phase flow of water and NAPL is described by the dimensionless Buckley–Leverett (BL) equation (Buckley & Leverett, 1942):

$$\phi \frac{\partial S_w}{\partial t_D} + \frac{\partial f_w}{\partial x_D} = 0 \tag{7}$$

where ϕ is porosity, S_w is the water saturation, f_w is the fractional flow of water, and t_D and x_D are the dimensionless distance and time parameters, respectively. The three latter parameters are defined by:

$$f_w = \frac{k_{\mathrm{rw}}/\mu_w}{k_{\mathrm{rw}}/\mu_w + k_{\mathrm{rn}}/\mu_n} \tag{8}$$

$$t_D = ut/\varphi L \tag{9}$$

$$x_D = x/L \tag{10}$$

where L is the porous medium length, t is the injection time, φ is the rock porosity and u denotes the injection Darcy velocity.

The transport of salt (C_s) in the aqueous phase for a two-phase system by neglecting dispersion, diffusion, and adsorption is described by:

$$\phi \frac{\partial (S_w C_s)}{\partial t_D} + \frac{\partial (f_w C_s)}{\partial x_D} = 0 \tag{11}$$

For a more comprehensive explanation, the readers are referred to Jerauld et al. (1984) and Pope (1980).

2.3. Shock Front Stability

Secondary and tertiary displacement refer to the injection of a fluid for enhancing the recovery of oil. In the secondary mode, the injected fluid is often "inert," that is, does not significantly change the existing rock-fluid equilibrium of the reservoir (even though reactive fluids such as SW are sometimes injected in secondary mode). The tertiary displacement method is usually applied to recover immobile oil by utilizing chemicals such as surfactants or MSW to change the wettability of the rock surface (Green & Willhite, 1987). Because the wettability alteration changes the shape of relative permeability curves (Mohammed & Babadagli, 2015), here, we select three sets of relative permeability curves to illustrate the impact of wettability alteration on shock front stability for both secondary and tertiary MSW flooding schemes. The relative permeability curves history-matched by Taheriotaghsara, Bonto, et al. (2020) and Taheriotaghsara, Hosseinzadehsadati, and Nick (2020) are used here. Various history matched core flooding observations (Ayirala et al., 2020; Dang et al., 2016; Nasralla et al., 2018; Sorop et al., 2015; Wang & Alvarado, 2016) obtain a similar behavior for relative permeability curves and conclude that changing the wettability from non-water-wet to water-wet condition shifts relative permeability curves of MSW to the right. Figure 1a depicts the relationship between the relative permeability of oleic and aqueous phases for water flooding with FW, SW, and a MSW (which is chosen as a 10 times diluted SW). Note that the secondary mode refers to the injection of MSW into a reservoir saturated with FW and NAPL. In contrast, the tertiary mode refers to the mobilization of residual NAPL by MSW flooding after the secondary displacement mode of SW injection (Figure S1 in Supporting Information S1).

Figure 2 displays the procedure of the analytical solution for finding the shock front saturation for both secondary and tertiary displacement methods for a 1D system. Despite the same shock front velocity of the MSW, the displaced brine flows with a different velocity from the secondary to tertiary MSW flooding methods. In the secondary mode, the line's slope between the intersection point (S_{w2}^{SEC}) and initial water saturation (S_{wi}) determines

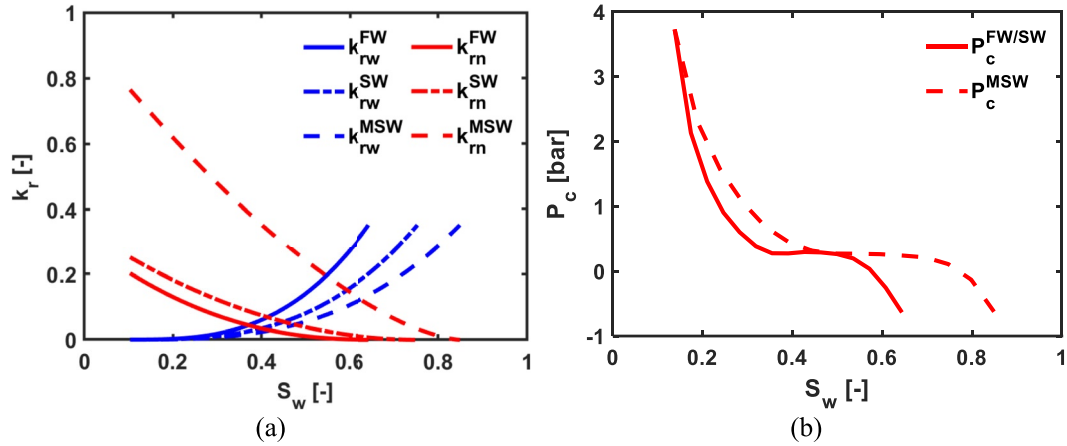

Figure 1. (a) Relative permeability for formation water (FW), seawater (SW), and modified salinity water (MSW) obtained from experimental data for carbonate rocks (Taheriotaghsara, Bonto, et al., 2020 and Taheriotaghsara, Hosseinzadehsadati, & Nick, 2020). (b) Capillary pressure for FW or SW and MSW water (we assume that the FW and SW display the same capillary pressure).

the saturation velocity of FW. However, the line's slope between the intersection point (S_{w2}^{TERT}) and residual NAPL saturation ($S_{\mathrm{nr}}^{\mathrm{SW}}$) controls the saturation velocity of SW in the tertiary displacement mode (Figure 2).

2.4. Front Dissipation

While neglecting the capillarity in the immiscible displacement of two-phase flow results in the formation of a sharp shock front, considering the capillarity causes a dissipated BL shock front. Laboratory efforts toward elucidating the influence of capillary pressure on the front stability were initiated by studies of Chuoke et al. (1959). They concluded that capillary pressure has a stabilizing influence on the shock front (i.e., preventing the occurrence of fingering). Many studies reported stability analyses of immiscible displacement in porous media by considering the capillarity in a one-dimensional domain (Babchin et al., 2008; Jerauld et al., 1984; Riaz & Tchelepi, 2004, 2006a; Yortsos & Hickernell, 1989). Capillarity changes a sharp shock front into a diffuse one with an extended tail. As a result, the mobility ratio at the shock front is reduced suppressing the instability (Berg

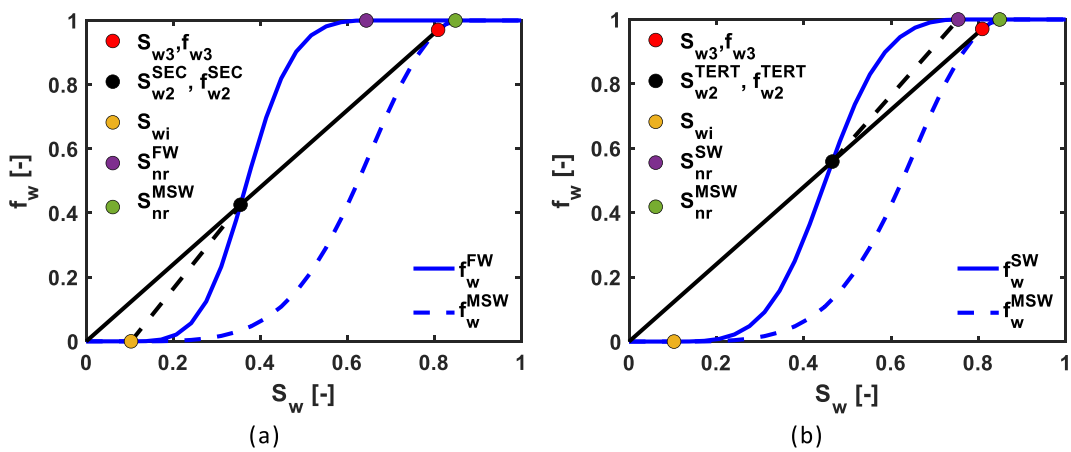

Figure 2. Construction of water fractional flow curves versus water saturation of modified salinity water (MSW) injection for (a) secondary (formation water) and (b) tertiary (seawater [SW]) displacement methods. The shock velocity of the modified salinity front is obtained by the slope of the tangent line to the modified salinity fractional flow curve (S_{w3}) ($= f_{w3}/S_{w3}$). The slope of intersecting lines (S_{w2}^{SEC} and S_{w2}^{TERT}) with initial water saturation (S_{wi}) and residual nonaqueous liquid saturation of SW ($S_{\mathrm{nr}}^{\mathrm{SW}}$) determines the shock velocity for secondary ($= f_{w2}^{\mathrm{SEC}} / \left(S_{w2}^{\mathrm{SEC}} - S_{\mathrm{wi}}\right)$) and tertiary ($= \left(1 - f_{w2}^{\mathrm{TERT}}\right) / \left(S_{\mathrm{nr}}^{\mathrm{SW}} - S_{w2}^{\mathrm{TERT}}\right)$) MSW flooding methods, respectively.

& Ott, 2012). Peters and Flock (1981) proposed a dimensionless number (I_{sc}) for the onset of instability in the cylindrical system, that is defined by

$$I_{sc} = \frac{(M-1)(v-v_c)\mu_w D^2}{C^* \sigma k_{wor}} \tag{12}$$

where M is the mobility ratio, v_c is the characteristic velocity, D is the diameter of the core, C^* is the wettability number, σ is the interfacial tension, and k is the absolute permeability. Equation 12 indicates that the capillary pressure smoothens sharp mobility contrast at the shock front of the fingers (Berg & Ott, 2012). Inclusion of capillarity, therefore, leads to a decrease in fingering by introducing dissipation in the flow (Al-Shalabi & Ghosh, 2018) and it depends on the domain's length scale (Berg & Ott, 2012; Yortsos & Hickernell, 1989). To take capillary pressure into account in this study, we use the capillary pressure curves (Figure 1b) used in Andrianov and Nick (2019) and adjust them to the corresponding values of residual saturation shown in Figure 1a.

2.5. Shock Front Mobility Ratio

Several studies propose various criteria for the onset of the front instability. In the case of no gravity and capillarity, a simple form of shock front mobility ratio, M_s, is expressed as (Rachford, 1964; Tang & Kovscek, 2011),

$$M_s = \frac{(k_{rw}/\mu_w)_{shock}}{(k_{rn}/\mu_n)_{+\infty}} \tag{13}$$

where $shock$ and $+\infty$ refer to the value at the shock front and maximum values of respective relative permeability curve at a location far downstream, respectively. The shock front total mobility ratio (M_s^T) has, however, been broadly accepted to assess the shock front stability (Hagoort, 1974; Jerauld et al., 1984; Riaz & Tchelepi, 2006a; Tripathi & Mohanty, 2008). A general form of total mobility ratio is expressed by,

$$M_s^T = \frac{(\lambda_T)_{shock}}{(\lambda_T)_{+\infty}} = \frac{(k_{rw}/\mu_w + k_{rn}/\mu_n)_{shock}}{(k_{rw}/\mu_w + k_{rn}/\mu_n)_{+\infty}} \tag{14}$$

where λ_T is total mobility. Both $M_s > 1$ and $M_s^T > 1$ conditions are commonly used for determining the onset of instability at the shock front. In this study, we use the total mobility ratio (M_s^T) to evaluate the onset of front instability because it includes the combination of both fluid phases on both sides of the shock front.

Considering MSW flooding, the saturation value at the shock front and the mobility ratio across the shock controls the stability of flow between MSW injection and displaced water (FW or SW) (Chorin, 1983; Hagoort, 1974). The saturation of the shock front depends on the shape of relative permeability curves. In order to evaluate the influence of relative permeability curves on the front stability, we define the shock total mobility ratio as a function of relative permeability functions. Assuming that NAPL and water viscosities are the same, the shock mobility ratio reads,

$$M_s^T = \frac{(\lambda_w+\lambda_n)_{S_{w3}}}{(\lambda_w+\lambda_n)_{S_{w2}}} = \frac{k_{rw,max}^{MSW}\left(\frac{S_{w3}-S_{wi}^{MSW}}{1-S_{wr}^{MSW}-S_{nr}^{MSW}}\right)^{n_w^{MSW}} + k_{rw,max}^{MS}\left(\frac{1-S_{w3}-S_{nr}^{MSW}}{1-S_{wi}^{MSW}-S_{nr}^{MSW}}\right)^{n_n^{MSW}}}{k_{rw,max}^{FW/SW}\left(\frac{S_{w2}-S_{wi}^{FW/SW}}{1-S_{wi}^{FW/SW}-S_{nr}^{FW/SW}}\right)^{n_w^{FW/SW}} + k_{rw,max}^{HS}\left(\frac{1-S_{w2}-S_{nr}^{FW/SW}}{1-S_{wi}^{FW/SW}-S_{nr}^{FW/SW}}\right)^{n_n^{FW/SW}}} \tag{15}$$

where S_{w3} and S_{w2} are obtained by drawing a tangent line to the modified salinity factional flow curve and the intersection of this line with the SW or FW fractional flow curve, respectively, as illustrated in Figure 2.

3. Model Configuration

A 1D model is utilized to determine the most affecting instability factors when the viscosity ratio is one. Similar to Kadeethum et al. (2019), we utilize the full factorial design (Sall et al., 2012) to explore the controlling factors. In this analysis, we take into account all relative permeability parameters for both modified and high salinities. Many studies (Morrow et al., 1998; Tang & Morrow, 1997; Webb et al., 2005) concluded from their

Table 1
Data Input for Full Factorial Design

	Parameters								
Level	n_w^{FW}	n_n^{FW}	$k_{rw,max}^{FW}$	$k_{rn,max}^{FW}$	S_{nr}^{FW}	S_{wi}^{FW}	n_w^{MSW}	n_n^{MSW}	$k_{rn,max}^{MSW}$
1	1	1	0.05	0.05	0.05	0.05	1	1	0.05
2	2	2	0.2	0.2	0.1	0.1	2	2	0.2
3	3	3	0.4	0.4	0.2	0.2	3	3	0.4
4	4	4	0.6	0.6	0.3	0.3	4	4	0.6
5	5	5	0.8	0.8	0.4	0.4	5	5	0.8
6	6	6	1	1	0.5	0.45	6	6	1

series of experiments on various reservoir systems that the water relative permeability at residual NAPL saturation remains constant, although residual NAPL saturation reduces due to wettability alteration. Therefore, in the present study, it is assumed that initial water saturation and water relative permeability of modified and high salinities are the same, and residual NAPL saturation reduction is a function of the wettability alteration intensity, which constrains the change of rock wettability from non-water-wet to water-wet condition. Table 1 lists the input parameters for the full factorial design, where levels 1 and six indicate the minimum and maximum values, respectively. Note that we only consider two levels for residual NAPL saturation of MSW ($S_{nr}^{MS} = 0.95S_{nr}^{FW}$ and $S_{nr}^{MS} = 0.8S_{nr}^{FW}$); hence, 2×6^9 BL analysis for immiscible two-phase flow are carried out in total. The JMP platform (Sall et al., 2012) is utilized to perform statistical analysis.

As shown in Figure S2 of Supporting Information S1, 2D and 3D models with a size of 200×80 m^2 and $200 \times 80 \times 80$ m^3 are designed for numerical analysis, respectively, bears a close resemblance to the one proposed by Hosseinzadehsadati et al. (2022a, 2022b). One should note that the grid blocks size has to be smaller than the wavelength of fingers to ensure numerical accuracy. However, it has a high computation cost in 3D; hence, we report the results mostly in 2D. Like Taheriotaghsara, Bonto, et al. (2020) and Taheriotaghsara, Hosseinzadehsadati, and Nick (2020), where they studied the mesh sensitivity of water breakthrough as a function of the block size for the same dimension reservoir, the 2D (3D) model is discretized by 500 grid blocks in the x-direction and 200 grid blocks in the y-direction (and 200 grid blocks in the z-direction). The same viscosity of 0.001 Pa.s and density of 1,000 kg/m^3 are considered for both water and NAPL Table S1 in Supporting Information S2). Similar to Tripathi and Mohanty (2008), an uncorrelated heterogeneous permeability field is used with a minimal standard variance of 0.05 and an average of 10 mD. The porosity is assumed to be uniform, with a value of 0.3. Note that the relative permeability curves of Figure 1a are used for the following simulations unless otherwise stated.

4. Results

Through this section, we discuss the onset of shock front instability due to wettability alteration under the influence of shock front total mobility ratio, relative permeability parameters, heterogeneity, capillary pressure, and role of secondary and tertiary injection of MSW.

4.1. Shock Front Instability in 1D Systems

Performing linear stability analyses for the immiscible displacement of BL equations, Riaz and Tchelepi (2004) concluded that the total mobility ratio above unity leads to unstable conditions across the saturation shock front. Similar to Riaz and Tchelepi (2006a) and Tripathi and Mohanty (2008), Figure 3 illustrates the total mobility profile of the fractional flow curves of secondary and tertiary displacement modes for the 1D model when the MSW injection alters the wettability of the rock surface. The differences between secondary and tertiary displacement modes for the given relative permeability curves are: (a) the secondary displacement mode refers to the injection of MSW into the reservoir saturated with FW and NAPL, whereas the tertiary displacement mode refers to injection of MSW after the secondary injection of SW aiming at mobilizing the residual NAPL; and, (b) the water saturation jumps from S_{wi} to S_{w2}^{SEC} in the secondary displacement mode while in the tertiary displacement mode it jumps from $1 - S_{nr}^{SW}$ to S_{w2}^{TERT}. Again, the viscosity of water and NAPL is equal to one in this example, and the relative permeability curves for FW and SW are different, as shown in Figure 1a. Moreover, S_{wi}, S_{w2}^{SEC}, and S_{w2}^{TERT} are independent of time.

Figure 3 shows the total mobility ratio across the modified salinity shock front in this example is about 3.2 and 2.8 for secondary and tertiary displacement methods, respectively. Hence, according to the shock front instability criteria (Equation 14), the shock front is unstable both in secondary and tertiary displacement modes due to the higher mobility of MSW caused by wettability alteration. There are no sharp interfaces (piston-like displacement)

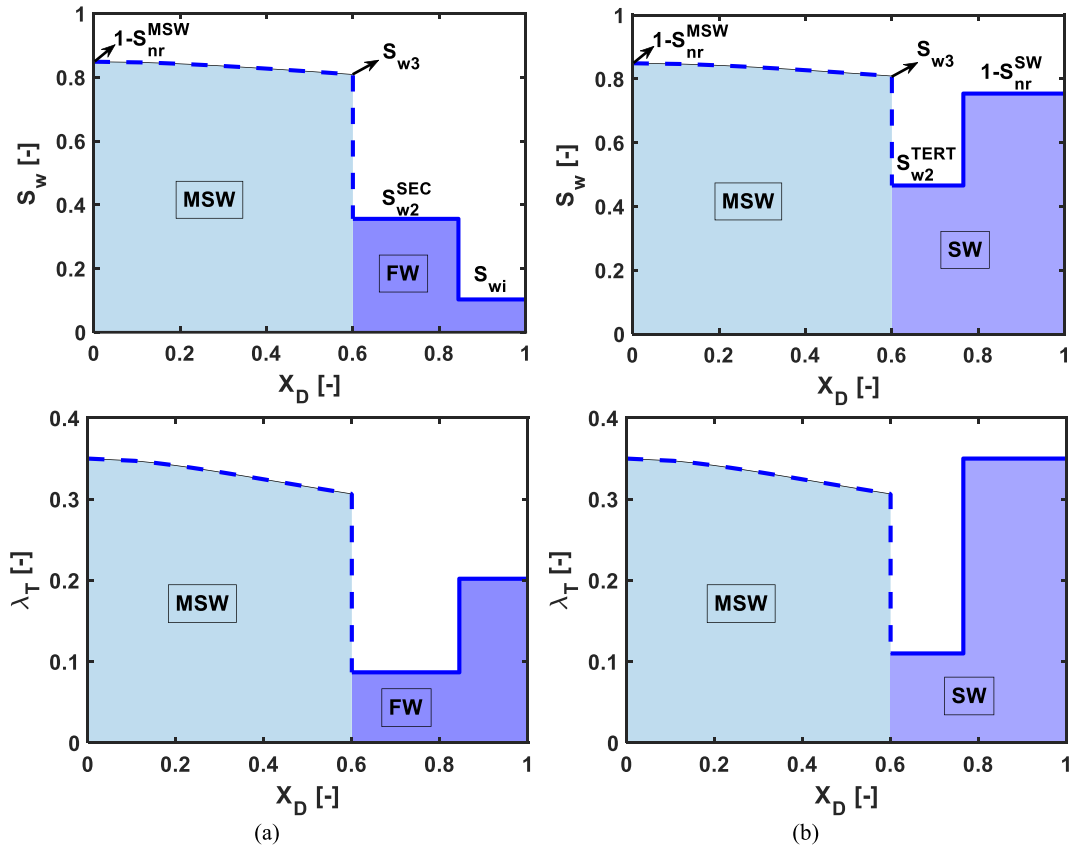

Figure 3. Saturation (S_w) and total mobility (λ_T) profiles after 0.5 pore volume injection of modified salinity water (MSW) (for the given relative permeability curves in Figure 1a) (a) secondary, (b) tertiary MSW flooding methods.

between displacing and displaced fluids in such a displacement. This is called the non-ideal displacement, which is typically more common in nature, and occurs when the total mobility ratio is above unity (Dake, 1983).

4.2. Impact of Mobility Ratio at the Shock Front in 2D Systems

In a stable condition at the shock front, an insignificant perturbation induced, for example, by permeability heterogeneity disappears with time. However, in an unstable condition, a small perturbation at the initial state results in a disturbance in the system that progresses with time (Drazin, 2002). Different mobility ratios at the shock front and its effect on the fluid flow are analyzed in a slightly heterogeneous media to evaluate the impact of wettability alteration on the shock front stability. Various total mobility ratios at the shock front are employed by the values of $M_s^T = 3.95$, $M_s^T = 2.65$, $M_s^T = 1.64$, and $M_s^T = 0.96$ to determine to what extent the generated fingers propagate at a large scale (relative permeability parameters are summarized in Table S2 in Supporting Information S2).

Figures 4a–4d) shows the saturation fields and contours for simulation of various aforementioned total mobility ratio after injecting 0.53 pore volume (PV) of modified salinity as the secondary mode. This is evident that the fingers are longer for the system with a higher total mobility ratio at the shock front. To compare the results with the BL solutions, the shock front obtained by the analytical solution (1D stable flooding) is shown by red dashed lines in Figures 4a–4d). By reducing the total shock front mobility ratio (M_s^T), the shock front of the 2D simulation approaches the 1D BL profile.

The intrinsic unstable characteristics of fingering indicate that a slight perturbation between fluid interfaces causes fingers to grow (Bakharev et al., 2020). As illustrated in Figure 5, a tiny perturbation of the displacement front (Figure 5a) at the initial stage of injection grows in time. Initially, a large number of fingers appear, while a few dominant fingers reach the outlet after injecting 0.47 PV of MSW (by merging the smaller ones). Therefore, the width of fingers increases throughout the displacement process in time. Figure 4e also displays

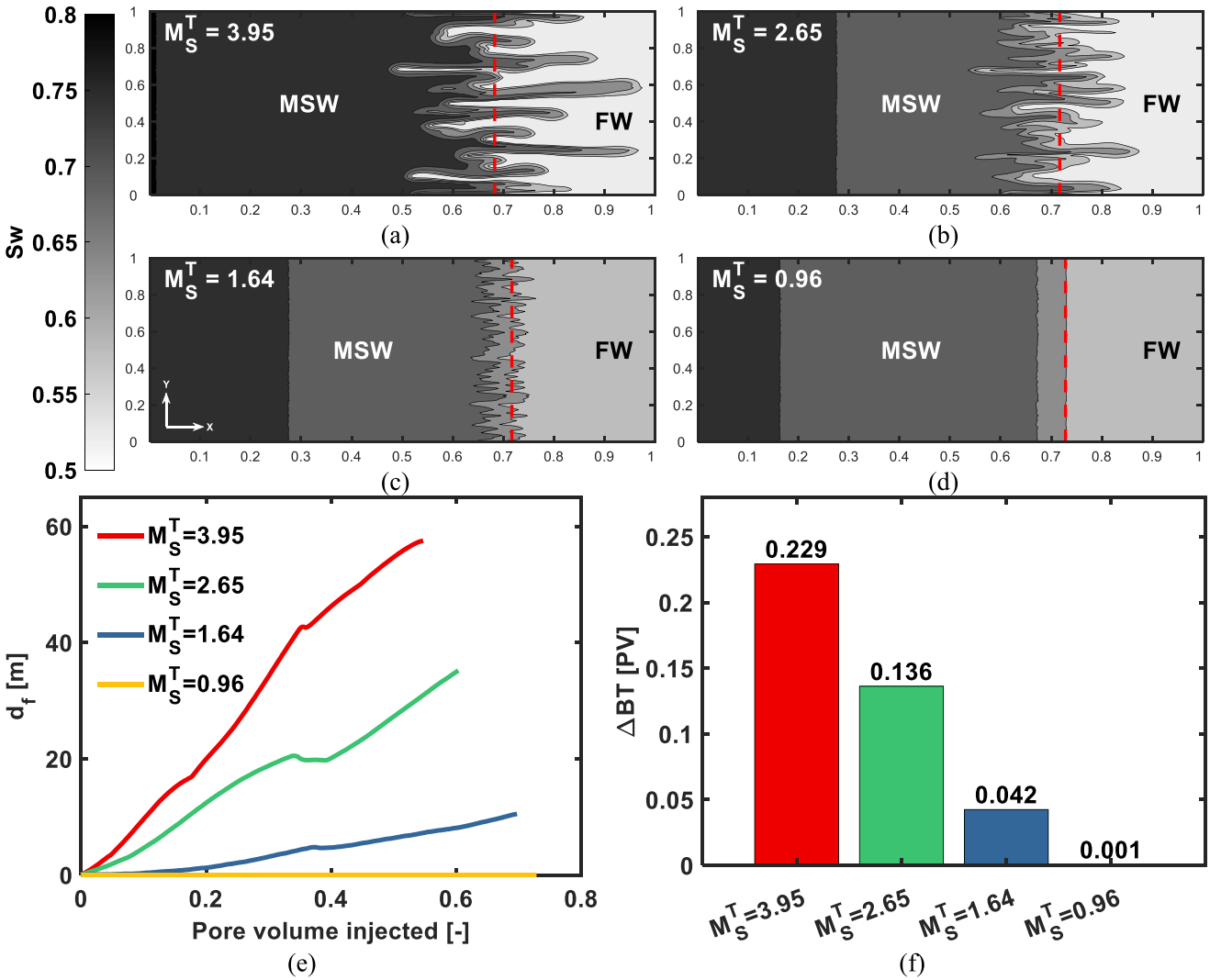

Figure 4. Water saturation fields during secondary displacement at 0.53 pore volume for (a) $M_s^T = 3.95$, (b) $M_s^T = 2.65$, (c) $M_s^T = 1.64$, and (d) $M_s^T = 0.96$ (see relative permeability parameters in Table S2 in Supporting Information S2). The red dashed line shows the shock front of modified salinity water from the Buckley–Leverett analytical solution. *X*- and *Y*-axis show the dimensionless length scale in *x*- and *y*-direction. (e) The distance between the tip of the most extended finger and analytical shock front (d_f). (f) Early breakthrough time due to the fingering effect compared with the stable (analytical) front (ΔBT).

that the distance between the most extended finger and the analytical solution of the shock front (d_f) grows with time. As shown in Figure 4e, for lower mobility ratio or mild fingering, the rate of growth of fingers is slow; particularly when $M_s^T = 0.96$, no growth is observed. Fingers cause bypassing of significant volumes of NAPL leading to an early breakthrough of MSW into outlet boundary (e.g., a production well). For example, for the case of $M_s^T = 3.95$, that is, a total mobility ratio of 3.95 across the front, the breakthrough of MSW flooding occurs almost 23% faster compared with the 1D BL profile (a stable front), here shown as ΔBT in Figure 4f. Early water breakthrough is unfavorable at the field scale because it leads to high brine flow into outlet.

4.3. Impact of Relative Permeability Parameters on Total Mobility Ratio in 1D Systems

A full factorial design is performed to rank relative permeability parameters for both modified and high salinities with the aim of finding the two-phase flow parameters resulting in instability due to wettability alteration. Throughout the present section, the 1D BL model is used to evaluate the value of the shock front mobility ratio by varying Corey's relative permeability parameters (Equation 15). Again, we presume that initial water saturation and water relative permeability are independent of salinity. Here, the reduction of residual NAPL saturation is a

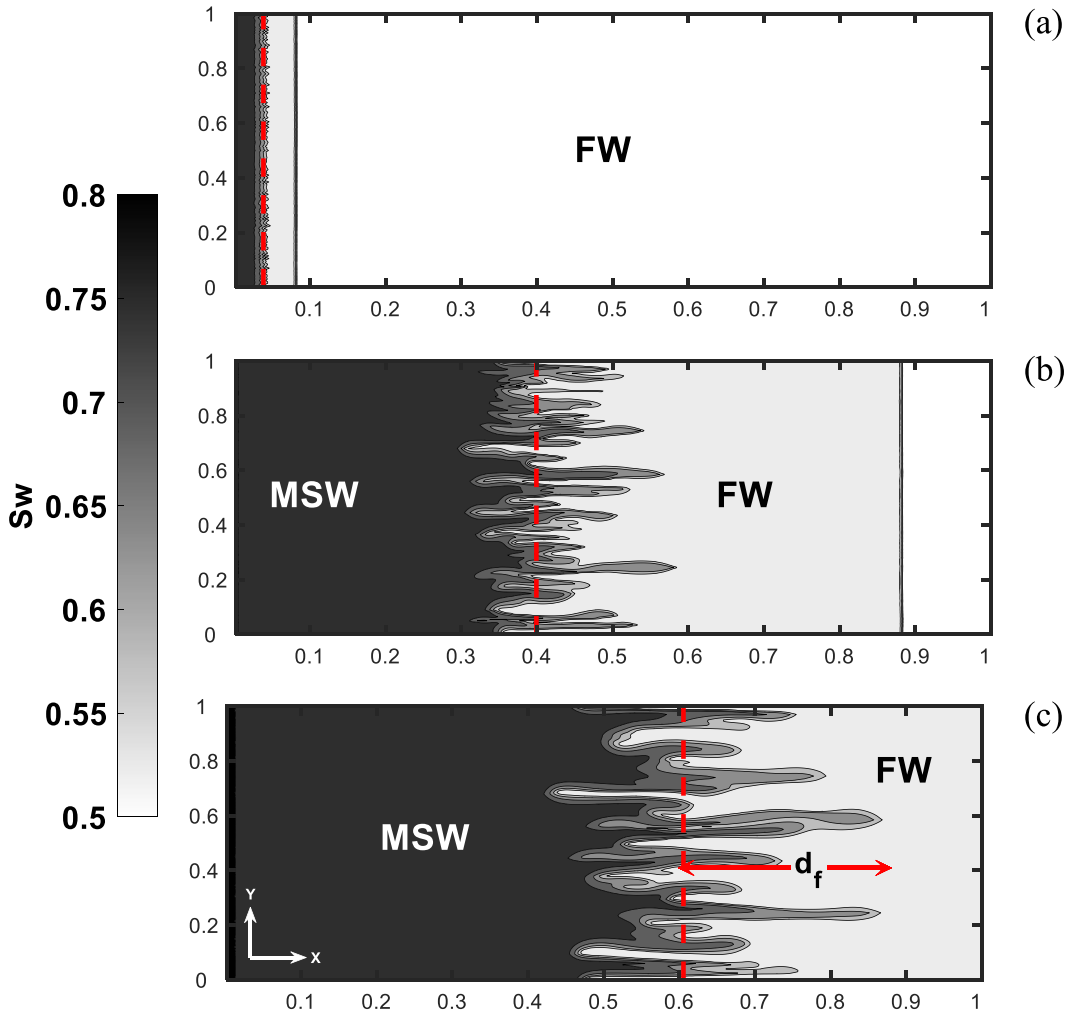

Figure 5. Water saturation profile of case $M_s^T = 3.95$ versus time (a) pore volume (PV) = 0.03, (b) PV = 0.31, (c) PV = 0.47. The red dashed line shows the shock front of modified salinity water obtained from the Buckley–Leverett analytical solution. *X*- and *Y*-axis show the dimensionless length scale in *x*- and *y*-direction.

function of the strength of altered wettability. Hence, the residual NAPL saturation of MSW is considered to be 5% and 20% lower than the residual NAPL saturation of FW.

Table S3 in Supporting Information S2 shows that all Corey's relative permeability parameters have a P-value less than 0.0001, implying that they significantly affect the onset of instability at the shock front. However, the impact of each parameter is different.

Figure 6 explains the estimated effect of each Corey's parameters as well as *t* ratio that represents the parameter effect on the shock front instability (Sall et al., 2012). For both cases, Corey's exponents of FW have the highest positive impact, while the maximum relative permeability of NAPL for FW has the highest negative impact. In other words, as Corey's exponents of FW become higher (or as the maximum relative permeability of NAPL with respect to FW becomes lower), the shock front instability develops faster. The observation is in line with Equation 14; it means that when the denominator (Equation 15) decreases, the mobility of the shock front increases, which in turn impacts the instability of the whole shock front.

The instability of the shock front in response to the residual NAPL saturation reduction due to wettability alteration is shown in Figure 6. It shows that the effect of each Corey's parameters remains constant except for Corey's exponents of MSW. Hence, by further reducing the residual NAPL saturation due to wettability alteration, the effect of water exponent becomes more important than NAPL exponent for the modified salinity relative permeability curves.

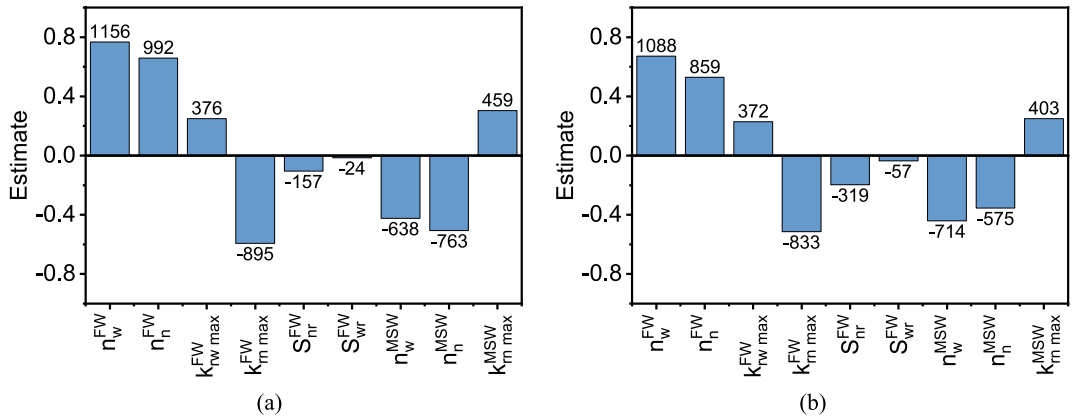

Figure 6. Estimated effect of each Corey's parameters for two scenarios (a) $S_{nr}^{MSW} = 0.8S_{nr}^{FW}$, (b) $S_{nr}^{MSW} = 0.95S_{nr}^{FW}$. The number on the top of each bar shows *t Ratio* (the difference between observed mean of the population to a theoretical value divided by standard error of the mean) implying the importance of each parameter. Positive and negative values imply directionality and reversal in the directionality of the effect, respectively. Each bar also contains a 95% confidence interval.

4.4. Impact of Relative Permeability Parameters With the Same Total Mobility Ratio in 2D Systems

In the previous section, we discussed the importance of the relative permeability curves to characterize the shock front stability. In this section, we compare the shape of the fingers under the same total mobility ratio but different relative permeability parameters. S2 case (Table S2 in Supporting Information S2) is considered as the reference case ($M_s^T = 2.65$) to show the influence of the relative permeability variations with the same total mobility ratio caused by wettability alteration. Figure 7 shows the water saturation distribution with different relative permeability sets after 0.59 PV injection, where all the total mobility ratio across the front is 2.65 for four different relative permeability sets. All relative permeability parameters are similar to S2, unless otherwise stated in Figure 7. The amplitude and the length of fingers for all cases are quite similar, leading more or less to the same breakthrough time, as illustrated in Figure 7. Therefore, the shape of the fingers is independent of relative permeability parameters for the same mobility ratio. However, the saturation distributions are different due to the various shape of the relative permeability curves.

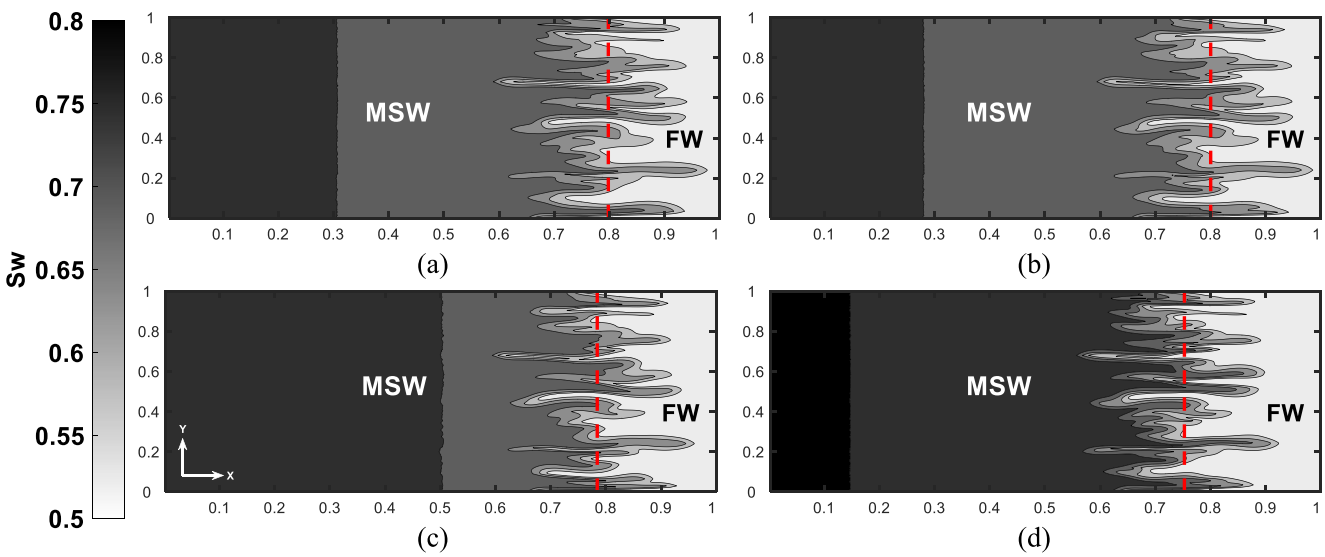

Figure 7. Water saturation profile during secondary mode at 0.59 pore volume for (a) S2 parameters (Table S2 in Supporting Information S2), (b) $k_{rn,max}^{MS} = 1$, $n_n^{MSW} = 2.84$, (c) $k_{rn,max}^{MS} = 1.0$, $n_w^{MSW} = 4.65$, $n_n^{MSW} = 2.6$, and (d) $n_w^{MS} = 3.8$, $S_{nr}^{MSW} = 0.15$. The red dashed line shows the shock front of modified salinity water by solving the analytical solution. *X*- and *Y*-axis show the dimensionless length scale in *x*- and *y*-direction. Buckley–Leverett solution and averaged saturation from (a to d) are plotted in Figure S3 in Supporting Information S1.

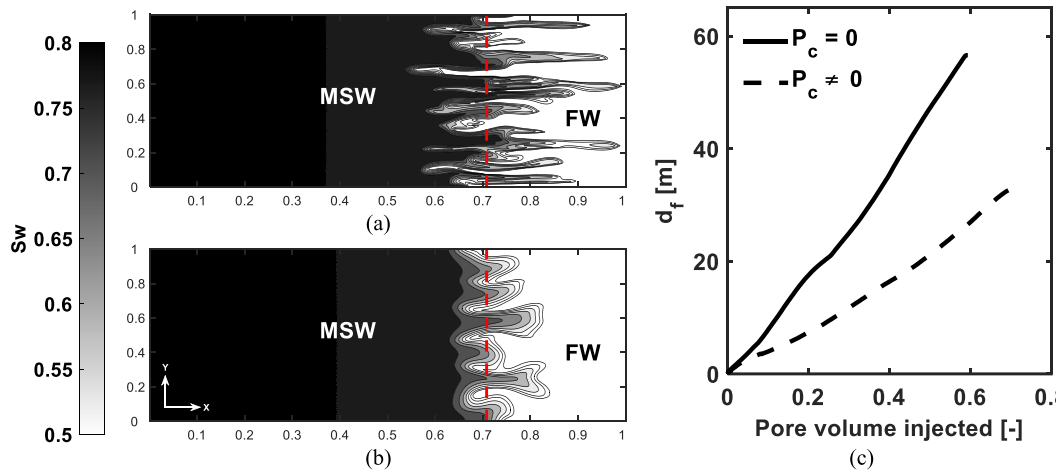

Figure 8. Water saturation profile during secondary displacement mode at 0.59 pore volume (PV) by using the relative permeability shown in Figure 1a (a) $P_c = 0$, (b) $P_c \neq 0$, and (c) the distance between the tip of the most extended finger and analytical shock front (d_f) versus PV injected in the presence and absence of capillary pressure.

4.5. Impact of Capillary Pressure in 2D Systems

For the field-scale calculations the flow rates are not sufficiently high for the viscous forces to be dominant; therefore, the inclusion of the capillary pressure is necessary (Firoozabadi & Aziz, 1991). They concluded that capillarity suppresses perturbation on short length scales more than those of larger scales. Therefore, the displacement at field scales could still be unstable. Figure 8a shows the unstable displacement in the absence of capillary pressure, where the relative permeability of Figure 1a for secondary injection is used. When capillary pressure is introduced to immiscible two-phase flow displacement, it transforms a sharp shock front into a diffuse zone. Therefore, the mobility contrast between displaced and displacing fluids decreases and the instability is suppressed similarly, as fingering in miscible displacements is counteracted by dispersion (Figure 8b). Figure 8c shows that the capillarity reduces the rates of fingers almost by half in this study. One should note that here we assume an immiscible displacement and no change of interfacial tension that can lead to wettability alteration.

4.6. Tertiary Injection of Modified Salinity Water in 2D Systems

For enhanced oil recovery, MSW flooding is applied both in secondary and tertiary displacement modes to reduce residual oil saturation by means of wettability alteration. In the current section, we examine the behavior of instability propagation during the tertiary displacement mode using the relative permeability of Figure 1a in the absence of capillary pressure.

In this example, the adverse mobility ratio across the shock front is not large during SW injection ($M_s^T = 1.8$); hence the slightly unstable saturation shock front takes place between SW and FW (Figure 9a). After 0.5 PV injection of SW, MSW is injected into the reservoir. However, due to the higher adverse mobility ratio between MSW and SW ($M_s^T = 2.8$) compared with SW and FW, fingers form longer than the secondary-mode injection of SW (Figure 9b). Fingers develop rapidly in the tertiary displacement mode because of the higher mobility ratio leading to steeper d_f versus PV injected, as shown in Figure 9c.

The average saturation from 2D simulations is compared with the BL solution in Figures 9d and 9e. The breakthrough time is 0.25 PV faster than the BL solution in tertiary displacement mode, while for the secondary mode, this value is 0.08 PV. In other words, the growth of fingers in tertiary displacement mode is nearly three times faster compared with the secondary mode, which causes an earlier water breakthrough.

4.7. Impact of Heterogeneity in 2D Systems

Several studies (Bakhshian et al., 2020; Nemer et al., 2021) show that the complex interplay between wettability and heterogeneity highly influences the fluid-fluid displacement patterns. However, all the previous simulations were performed using the standard deviation of 0.05 for generating an uncorrelated heterogeneous permeability

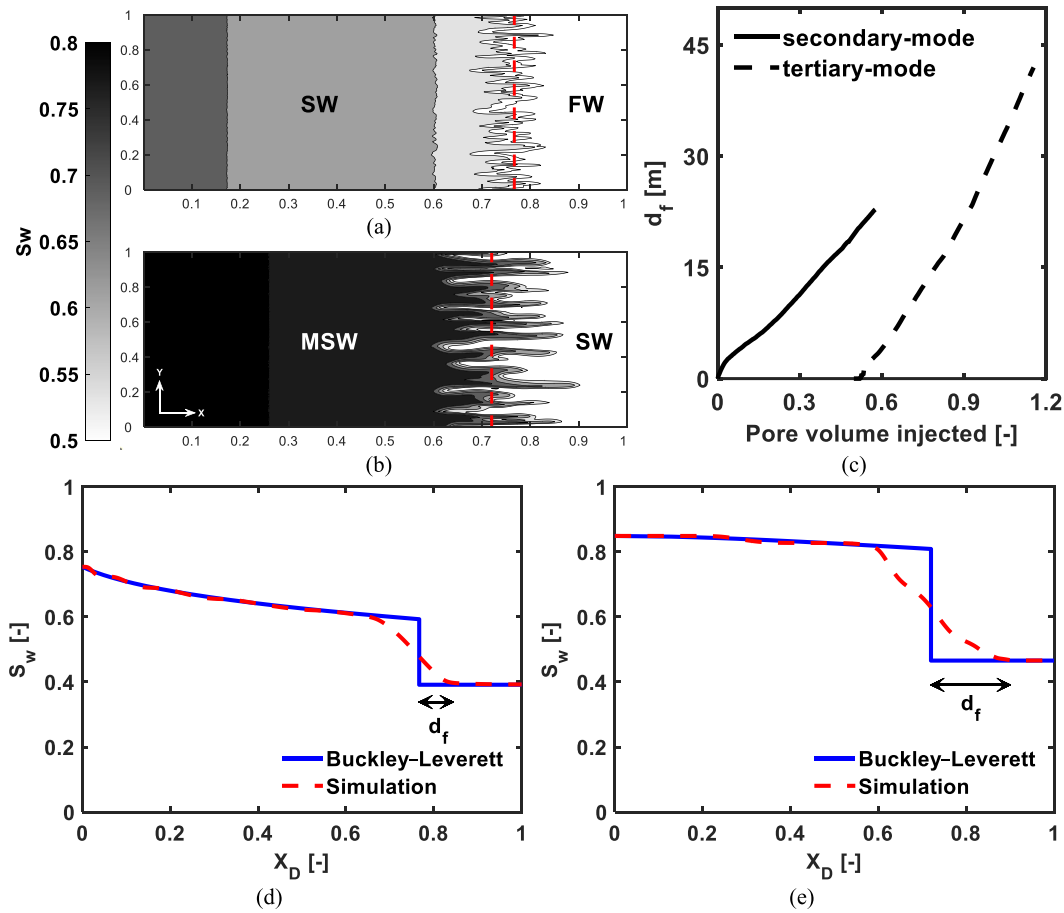

Figure 9. Water saturation profile during (a) secondary-mode injection of seawater (SW) at 0.5 pore volume (PV) by using the relative permeability shown in Figure 1a. (b) Tertiary displacement mode injection of modified salinity water (MSW) at 1.1 PV. (c) The distance between the tip of the most extended finger and analytical shock front (d_f) versus PV injected for secondary and tertiary displacement mode injection (d and e) Buckley–Leverett solution and averaged saturation from 2D simulation. (d) Secondary-mode injection of SW at 0.5 PV. (e) Tertiary displacement mode injection of MSW at 1.1 PV after injecting 0.5 of SW (the same approach is used for the calculation of d_f shown in this figure).

field, where the permeability varies between 9 and 11 mD (almost homogeneous). The standard deviation of 0.5 is used in the present section, and the permeability ranges between 7 and 13 mD to observe finger patterns caused by wettability alteration in a more heterogeneous porous medium. Figure 10 shows the water saturation distribution under the two aforementioned standard deviations. It is evident that the fingers associated with a higher standard deviation are slightly longer (Figure 10c) and thicker (Figures 10a and 10b). One could conclude that the extension of fingers is due to the channeling effect caused by the heterogeneity of porous media (Luo et al., 2018).

4.8. Front Stability in 3D Systems

For the 3D model, fine-grid numerical simulation with low heterogeneity is carried out to ensure that the grid blocks are smaller than the typical wavelength of the fingers to capture the phenomenon. The NAPL removal efficiency and water cut from 3D simulations (with and without capillary pressure) along with the BL analytical solution are shown in Figure 11. Figures 11a and 11b show a delayed NAPL removal efficiency and an earlier MSW breakthrough immediately after FW, respectively; these effects are observed because of fingering growth at the shock front caused by wettability alteration. Such effects are relaxed by including capillary pressure, as previously observed in 2D simulations. Figure 12 illustrates many same-sized fingers that are observed in 3D simulations in contrast to 2D simulations, where fewer dominant fingers were evolved because of less dispersion compared to 3D models. However, the impact of including the capillary pressure in the 3D simulations resulted

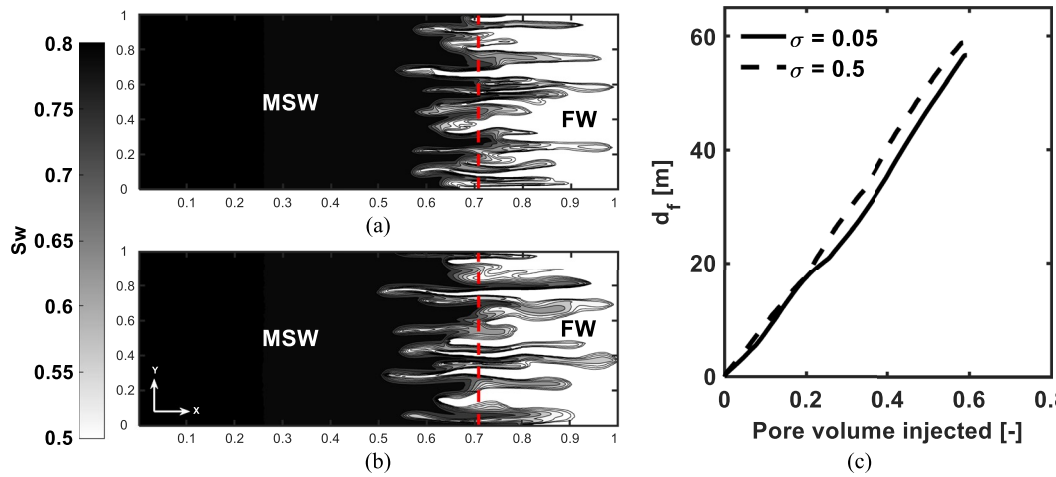

Figure 10. Water saturation profile during secondary mode at 0.59 pore volume (PV) (by using the relative permeability shown in Figure 1a) (a) $\sigma = 0.05$, (b) $\sigma = 0.5$, and (c) the distance between the tip of the most extended finger and analytical shock front (d_f) versus PV injected for $\sigma = 0.05$ and $\sigma = 0.5$.

in a lower degree of perturbation at the front. In the presence of capillary pressure, Figure 12c shows that some fingers evolve faster around the outlet where pressure drop is significant and reduces the impact of capillary pressure.

5. Discussion

Wettability alteration occurs as a result of the interactions between the brine/crude NAPL/rock interfaces. However, for field-scale reservoir simulation, the microscopic interface interactions are simplified to two sets of relative permeability curves (before and after interactions). Such relative permeability curves are obtained by history matching of core flooding experiments. This study shows that changing the wettability from non-water-wet to water-wet may cause instability at the shock front interface even for the same viscosity contrast. Fingering instability formed at the shock front depends entirely on the shape of the new relative permeability curve caused by wettability alteration. However, the finger's length is a function of the total mobility ratio across the shock front. Figure 13a reveals that the distance between most extended finger length and analytical solution (d_f) at the breakthrough time and the difference of breakthrough time between simulation and analytical solution (ΔBT) linearly increases as the mobility ratio increases. One should note that d_f is not equal to ΔBT because d_f represents the distance of numerical and analytical solutions at the breakthrough time (observed in numerical simulations),

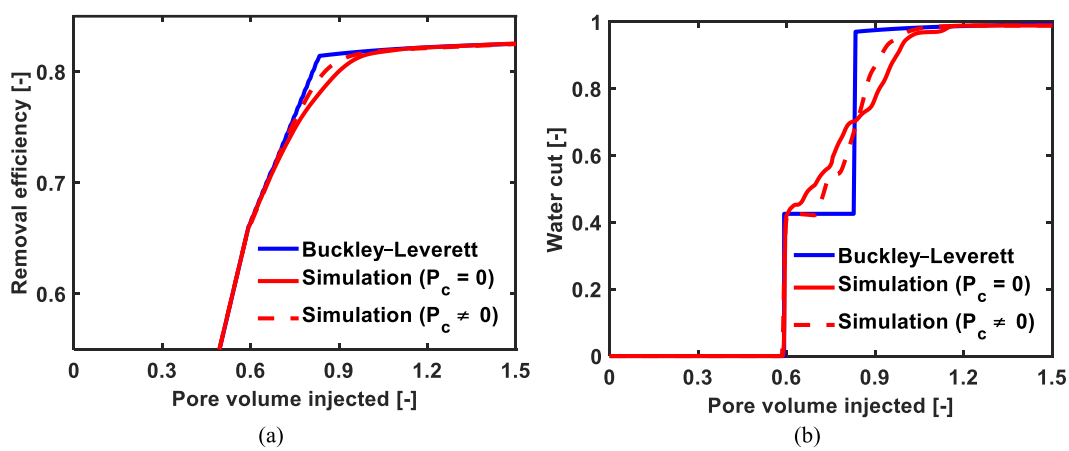

Figure 11. Comparison of Buckley–Leverett theory, simulation with and without P_c for (a) nonaqueous liquid removal efficiency and (b) water cut (the ratio of produced water to the total volume of produced liquids) during secondary injection mode of modified salinity water.

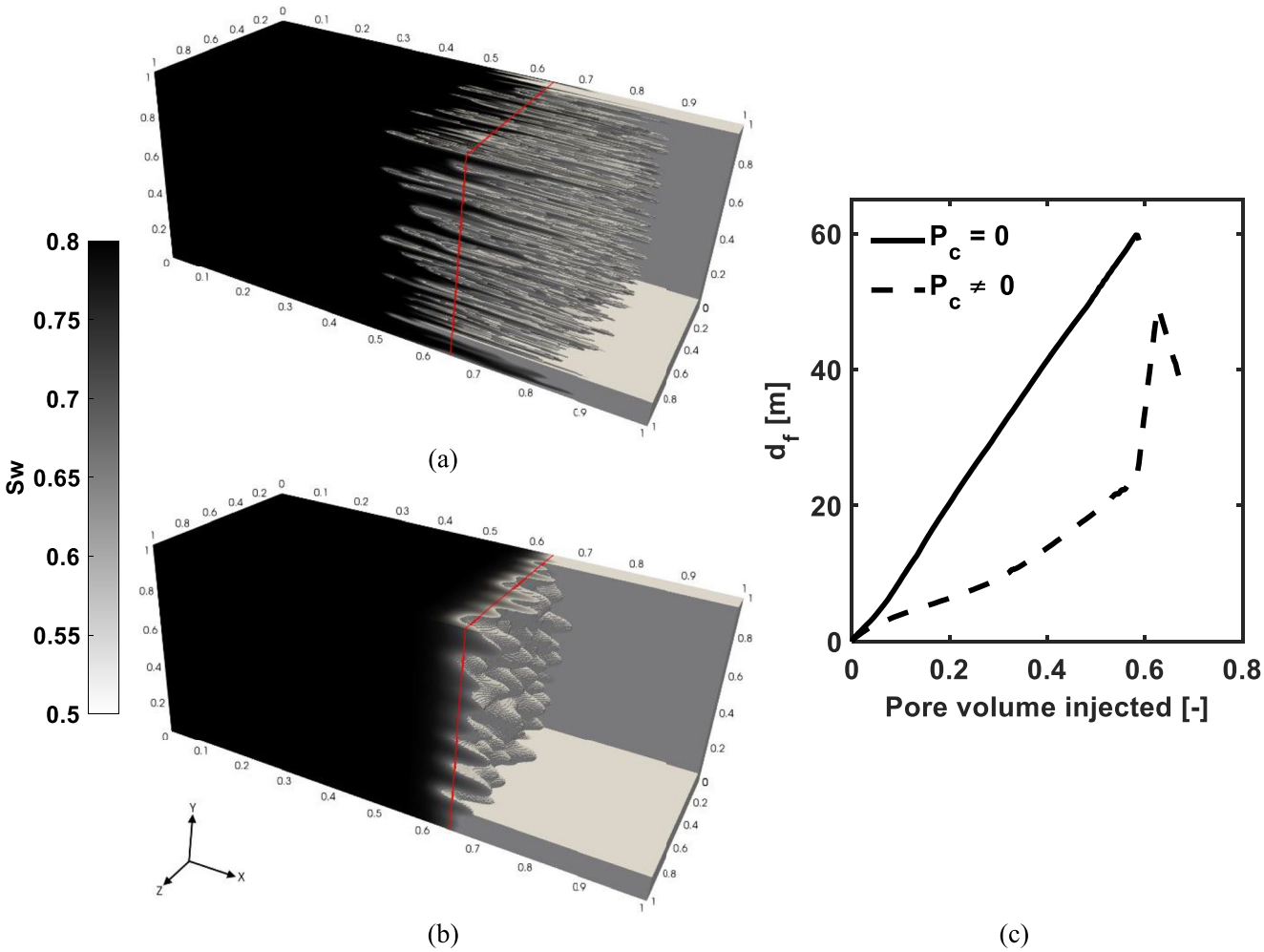

Figure 12. The water saturation distribution between inlet and outlet at 0.53 pore volume (PV) (by using the relative permeability shown in Figure 1a). (a) $P_c = 0$. (b) $P_c \neq 0$. (c) The distance between the tip of the most extended finger and analytical shock front (d_f) versus PV injected in the presence and absence of capillary pressure. The axis values show the dimensionless length scale in *x*-, *y*-, and *z*-direction. The red solid line shows the shock front of modified salinity water by solving the Buckley–Leverett analytical solution.

while ΔBT denotes the difference between the breakthrough time of numerical and analytical solutions. Since the velocity at the fingertip is higher than that of shock front analytical solution, d_f deviates from ΔBT for a high total mobility ratio. However, these two points meet when the total mobility ratio is one. Also, the tendency shows no difference in whether the water is injected as secondary or tertiary displacement mode for enhanced oil recovery purpose. Figure 13a shows that d_f and ΔBT decrease approximately by a factor of two due to the capillarity effect on the shock front dissipation. As stated before, the larger is the capillarity, the more stable the displacement becomes.

It is generally accepted that fingering instabilities are a three-dimensional process (Johannsen et al., 2006; Knorr et al., 2016; Pau et al., 2010). Finger length may decrease in 3D systems owing to more substantial dispersion than 2D systems; however, they may evolve thicker and more extended because of more available space for fingers to merge. The simulations conducted in this study show that the unstable shock front in 3D simulations differs widely in terms of finger density and pattern evolution compared with those of the 2D simulation. Nevertheless, the difference in d_f between 2D and 3D simulations in the presence and absence of capillary pressure is small (Figure 13b), resulting in no significant variation in the onset of instabilities. Still, whether the flow is 2D or 3D, the capillarity lowers the length of the fingers.

As mentioned before, viscosity of water and NAPL is considered equal in this study. However, the NAPL viscosity is generally higher than water viscosity; hence, the mobilized NAPL by MSW flooding causes an even higher

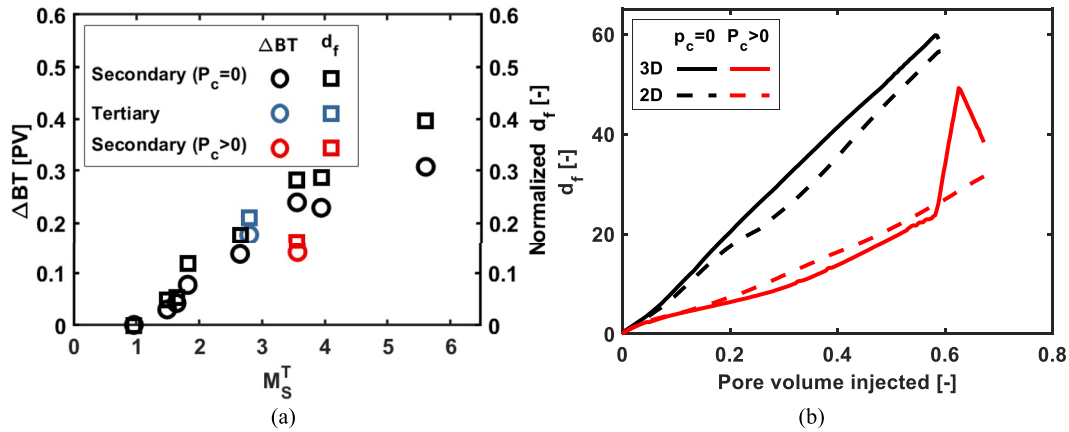

Figure 13. Summarized information of all simulation data obtained in this study. (a) The behavior of the distance between the tip of the most extended finger and analytical shock front for various cases (d_f) at breakthrough time and its early breakthrough time compared with analytical solution (ΔBT) versus total mobility ratio for secondary and tertiary displacement mode. (b) Calculated d_f in the presence and absence of capillary pressure in 3D (solid line) and 2D (dashed line) when the relative permeability of Figure 1a is used.

mobility ratio upstream at the MSW shock front (compared to the results of this study). Such effects at the shock fronts augment the unstable conditions that are neglected in field-scale simulations. Moreover, the stability of the shock front can be even more pronounced when there is a density gradient between NAPL and water, accompanied by the heterogeneity of the reservoirs.

It is quite a significant challenge for engineers to capture fingering and channeling at reservoir scale simulations where the grid blocks are relatively larger than the viscous finger wavelength (Luo et al., 2018). Therefore, the predicted NAPL removal efficiency at the field scale might be overestimated because fingers exist at a small scale. Blunt et al. (1994) developed a model for the fingering effect in multi-component systems by modifying the concentration and water saturation profile in a 1D analytical solution. Several studies (Adam et al., 2017; Chang et al., 1994; Luo et al., 2018; Tchelepi & Orr, 1994) have also revealed that the fingering can be ignored for considerable heterogeneity correlation length when the flow is dominated by channeling at the field scale. However, Luo et al. (2018) developed a model to scale up fingering effects where fingering and channeling coexist in the field. The applicability of their model can be investigated for the fingering caused by wettability alteration for future work.

6. Conclusions

This study presents systematic analyses of the stability characteristics of immiscible two-phase flow where the wettability alteration due to modified salinity, surfactant injection, or increasing temperature of injection fluid causes the growth of fingers even in the absence of viscosity contrast. Our observations are summarized as follows:

- The more wettability alteration toward the wetting phase (usually water-wet) is, the more unstable the shock front becomes. There may be a considerably unstable condition in the porous media if the total mobility ratio across the front is larger than 2.
- The relative permeability curve parameters due to wettability alteration have a different impact on instability. In particular, Corey's exponents and the maximum relative permeability of non-water-wet phase for FW have the highest impact on total mobility ratio. However, the shape of the fingers is independent of relative permeability parameters for the same mobility ratio.
- A substantial change of wettability toward the wetting phase leads to an early water breakthrough. For instance, the total mobility ratio of 3.95 at the shock front gives rise to 23% earlier breakthrough compared with the stable condition.
- The heterogeneity is an amplifying parameter that causes the enlargement of fingers' thickness than length
- From 3D simulations, the fingering effects become considerable in terms of NAPL removal efficiency and water cut.

- Although the length of the fingers is more or less similar in 3D and 2D, finger density and pattern are significantly dissimilar.
- The early breakthrough of MSW flooding is an unfavorable consequence of the wettability-induced fingering in the tertiary displacement mode at the field scale because it causes a delay in removal NAPL and increases the water cut.

Data Availability Statement

Data were interpreted using the commercial software Schlumberger ECLIPSE 100 (https://www.software.slb.com/products/eclipse/simulators), version 2019.1. A donation request form is available from Schlumberger for academic/research institutions at Software Donation Request (https://www.software.slb.com/softwaredonationform). Data sets related to this article can also be found at Hosseinzadehsadati et al., 2022b, https://doi.org/10.11583/DTU.17728562, an open-source online data repository hosted at Technical University of Denmark (DTU) data. Publicly accessible data will be available through the DTU data link upon publication, and the temporary link for the purposes of peer review can be found at https://figshare.com/s/e200d64de4482366173a.

Acknowledgments
The research leading to these results has received funding from the Danish Offshore Technology Center under the Advanced Water Flooding program.

References

Adam, A., Pavlidis, D., Percival, J. R., Salinas, P., De Loubens, R., Pain, C. C., et al. (2017). *Dynamic mesh adaptivity for immiscible viscous fingering*. Society of Petroleum Engineers - SPE Reservoir Simulation Conference (pp. 788–802). https://doi.org/10.2118/182636-MS

Al-Ibadi, H., Stephen, K. D., & Mackay, E. (2021). Pulse generation and propagation in the numerical solution of low salinity water flooding. *Journal of Petroleum Science and Engineering*, *198*, 108151. https://doi.org/10.1016/j.petrol.2020.108151

Al-Shalabi, E. W., & Ghosh, B. (2018). Flow visualization of fingering phenomenon and its impact on waterflood oil recovery. *Journal of Petroleum Exploration and Production Technology*, *8*(1), 217–228. https://doi.org/10.1007/s13202-017-0336-0

An, S., Erfani, H., Godinez-Brizuela, O. E., & Niasar, V. (2020). Transition from viscous fingering to capillary fingering: Application of GPU-based fully implicit dynamic pore network modeling. *Water Resources Research*, *56*(12), e2020WR028149. https://doi.org/10.1029/2020WR028149

Anderson, W. G. (1987). Wettability literature survey - Part 5: The effects of wettability on relative permeability. *JPT, Journal of Petroleum Technology*, *39*(11), 1453–1468. https://doi.org/10.2118/16323-PA

Andrianov, N., & Nick, H. M. (2019). Modeling of waterflood efficiency using outcrop-based fractured models. *Journal of Petroleum Science and Engineering*, *183*, 106350. https://doi.org/10.1016/j.petrol.2019.106350

Ayirala, S., Alghamdi, A., Gmira, A., Cha, D. K., Alsaud, M. A., & Yousef, A. (2020). Linking pore scale mechanisms with macroscopic to core scale effects in controlled ionic composition low salinity waterflooding processes. *Fuel*, *264*, 116798. https://doi.org/10.1016/j.fuel.2019.116798

Babchin, A., Brailovsky, I., Gordon, P., & Sivashinsky, G. (2008). Fingering instability in immiscible displacement. *Physical Review E*, *77*(2). 026301. https://doi.org/10.1103/physreve.77.026301

Bakharev, F., Campoli, L., Enin, A., Matveenko, S., Petrova, Y., Tikhomirov, S., & Yakovlev, A. (2020). Numerical investigation of viscous fingering phenomenon for raw field data. *Transport in Porous Media*, *132*(2), 443–464. https://doi.org/10.1007/s11242-020-01400-5

Bakhshian, S., Rabbani, H. S., Hosseini, S. A., & Shokri, N. (2020). New insights into complex interactions between heterogeneity and wettability influencing two-phase flow in porous media. *Geophysical Research Letters*, *47*(14), e2020GL088187. https://doi.org/10.1029/2020GL088187

Bear, J. (1972). *Dynamics of fluids in porous media* . American Elsevier Publishing Company. Retrieved from https://books.google.dk/books/about/Dynamics_of_Fluids_in_Porous_Media.html?id=9JVRAAAAMAAJ%26redir_esc=y

Berg, S., & Ott, H. (2012). Stability of CO2–brine immiscible displacement. *International Journal of Greenhouse Gas Control*, *11*, 188–203. https://doi.org/10.1016/j.ijggc.2012.07.001

Birkholzer, J., & Tsang, C. F. (1997). Solute channeling in unsaturated heterogeneous porous media. *Water Resources Research*, *33*(10), 2221–2238. https://doi.org/10.1029/97WR01209

Blunt, M. J., Barker, J. W., Rubin, B., Mansfield, M., Culverwell, I. D., & Christie, M. A. (1994). Predictive theory for viscous fingering in compositional displacement. *SPE Reservoir Engineering*, *9*(01), 73–80. https://doi.org/10.2118/24129-PA

Brooks, R., & Corey, A. (1966). Properties of porous media affecting fluid flow. *Journal of the Irrigation and Drainage Division*, *92*(2), 61–90. https://doi.org/10.1061/jrcea4.0000425

Buckley, S. E., & Leverett, M. C. (1942). Mechanism of fluid displacement in sands. *Transactions of the AIME*, *146*(01), 107–116. https://doi.org/10.2118/942107-g

Chang, Y. B., Lim, M. T., Pope, G. A., & Sepehrnoori, K. (1994). CO2 flow patterns under multiphase flow: Heterogeneous field-scale conditions. *SPE Reservoir Engineering*, *9*(03), 208–216. https://doi.org/10.2118/22654-PA

Chen, Y. F., Fang, S., Wu, D. S., & Hu, R. (2017). Visualizing and quantifying the crossover from capillary fingering to viscous fingering in a rough fracture. *Water Resources Research*, *53*(9), 7756–7772. https://doi.org/10.1002/2017WR021051

Chorin, A. J. (1983). The instability of fronts in a porous medium. *Communications in Mathematical Physics*, *91*(1), 103–116. https://doi.org/10.1007/BF01206054

Christie, M. A., & Bond, D. J. (1987). Detailed simulation of unstable processes in miscible flooding. *SPE Reservoir Engineering*, *2*(04), 514–522. https://doi.org/10.2118/14896-PA

Chuoke, R. L., van Meurs, P., & van der Poel, C. (1959). The instability of slow, immiscible, viscous liquid-liquid displacements in permeable media. *Transactions of the AIME*, *216*(01), 188–194. https://doi.org/10.2118/1141-g

Dake, L. (1983). *Fundamentals of reservoir engineering*. Elsevier. https://doi.org/10.1016/b978-088415643-7/50009-1

Dang, C., Nghiem, L., Nguyen, N., Chen, Z., & Nguyen, Q. (2016). Mechanistic modeling of low salinity water flooding. *Journal of Petroleum Science and Engineering*, *146*, 191–209. https://doi.org/10.1016/j.petrol.2016.04.024

Drazin, P. G. (2002). *Introduction to hydrodynamic stability*. Cambridge University Press. https://doi.org/10.1017/cbo9780511809064

Dullien, F. A. L. (1979). Porous media: Fluid transport and pore structure. *Dairy Science & Technology* (pp.551–659). CRC Taylor & Francis Group.
Farthing, M. W., Seyedabbasi, M. A., Imhoff, P. T., & Miller, C. T. (2012). Influence of porous media heterogeneity on nonaqueous phase liquid dissolution fingering and upscaled mass transfer. *Water Resources Research*, *48*(8), 8507. https://doi.org/10.1029/2011WR011389
Firoozabadi, A., & Aziz, K. (1991). Relative permeabilities from centrifuge data. *Journal of Canadian Petroleum Technology*, *30*(05), 33. https://doi.org/10.2118/91-05-02
Glass, R. J., Parlange, J.-Y., & Steenhuis, T. S. (1989). Wetting front instability: 1. Theoretical discussion and dimensional analysis. *Water Resources Research*, *25*(6), 1187–1194. https://doi.org/10.1029/WR025I006P01187
Gorell, S. B., & Homsy, G. M. (1983). A theory of the optimal policy of oil recovery by secondary displacement processes. *SIAM Journal on Applied Mathematics*, *43*(1), 79–98. https://doi.org/10.1137/0143007
Green, D. W., & Willhite, G. P. (1987). Enhanced oil recovery. *Developments in Petroleum Science*, *21*(C), 1–35. https://doi.org/10.1016/S0376-7361(08)70369-8
Hagoort, J. (1974). Displacement stability of water drives in water-wet connate-water-bearing reservoirs. *Society of Petroleum Engineers Journal*, *14*(01), 63–74. https://doi.org/10.2118/4268-PA
Homsy, G. M. (1987). Viscous fingering in porous media. *Annual Review of Fluid Mechanics*, *19*(1), 271–311. https://doi.org/10.1146/annurev.fl.19.010187.001415
Hosseinzadehsadati, S., Eftekhari, A. A., & Nick, H. M. (2022a). Role of relative permeability hysteresis in modified salinity water flooding. *Fuel*, *321*, 124085. 10.1016/j.fuel.2022.124085
Hosseinzadehsadati, S., Eftekhari, A. A., & Nick, H. M. (2022b). Data for "Impact of wettability alteration on the front instability of immiscible displacement in porous media" paper. [Dataset]. Technical University of Denmark. 10.11583/DTU.17728562
Jerauld, G. R., Davis, H. T., & Scriven, L. E. (1984). Stability fronts of permanent form in immiscible displacement. In *SPE Annual Technical Conference and Exhibition*. Society of Petroleum Engineers. https://doi.org/10.2118/13164-MS
Jerauld, G. R., Lin, C. Y., Webb, K. J., & Seccombe, J. C. (2008). Modeling low-salinity waterflooding. *SPE Reservoir Evaluation and Engineering*, *11*(06), 1000–1012. https://doi.org/10.2118/102239-PA
Johannsen, K., Oswald, S., Held, R., & Kinzelbach, W. (2006). Numerical simulation of three-dimensional saltwater–freshwater fingering instabilities observed in a porous medium. *Advances in Water Resources*, *29*(11), 1690–1704. https://doi.org/10.1016/J.ADVWATRES.2005.12.008
Kadeethum, T., Salimzadeh, S., & Nick, H. M. (2019). An investigation of hydromechanical effect on well productivity in fractured porous media using full factorial experimental design. *Journal of Petroleum Science and Engineering*, *181*, 106233. https://doi.org/10.1016/j.petrol.2019.106233
Karadimitriou, N. K., Mahani, H., Steeb, H., & Niasar, V. (2019). Nonmonotonic effects of salinity on wettability alteration and two-phase flow dynamics in PDMS micromodels. *Water Resources Research*, *55*(11), 9826–9837. https://doi.org/10.1029/2018WR024252
Kassa, A. M., Gasda, S. E., Kumar, K., & Radu, F. A. (2021). Modeling of relative permeabilities including dynamic wettability transition zones. *Journal of Petroleum Science and Engineering*, *203*, 108556. https://doi.org/10.1016/j.petrol.2021.108556
Khishvand, M., Alizadeh, A. H., Oraki Kohshour, I., Piri, M., & Prasad, R. S. (2017). In situ characterization of wettability alteration and displacement mechanisms governing recovery enhancement due to low-salinity waterflooding. *Water Resources Research*, *53*(5), 4427–4443. https://doi.org/10.1002/2016WR020191
Knorr, B., Xie, Y., Stumpp, C., Maloszewski, P., & Simmons, C. T. (2016). Representativeness of 2D models to simulate 3D unstable variable density flow in porous media. *Journal of Hydrology*, *542*, 541–551. https://doi.org/10.1016/J.JHYDROL.2016.09.026
LaForce, T., & Johns, R. T. (2005). Analytical solutions for surfactant-enhanced remediation of nonaqueous phase liquids. *Water Resources Research*, *41*(10), 10420. https://doi.org/10.1029/2004WR003862
Lake, L. W. (1989). *Enhanced oil recovery*. Prentice Hall. Retrieved from https://books.google.dk/books/about/Enhanced_Oil_Recovery.html?id=nm5MAQAAIAAJ%26redir_esc=y
Luo, H., Delshad, M., Pope, G. A., & Mohanty, K. K. (2018). Scaling up the interplay of fingering and channeling for unstable water/polymer floods in viscous-oil reservoirs. *Journal of Petroleum Science and Engineering*, *165*, 332–346. https://doi.org/10.1016/j.petrol.2018.02.035
Mahani, H., Keya, A. L., Berg, S., & Nasralla, R. (2017). Electrokinetics of carbonate/brine interface in low-salinity waterflooding: Effect of brine salinity, composition, rock type, and pH on ζ-Potential and a surface-complexation model. *SPE Journal*, *22*(01), 53–68. https://doi.org/10.2118/181745-PA
Mohammed, M., & Babadagli, T. (2015). Wettability alteration: A comprehensive review of materials/methods and testing the selected ones on heavy-oil containing oil-wet systems. *Advances in Colloid and Interface Science*, *220*, 54–77. https://doi.org/10.1016/j.cis.2015.02.006
Morrow, N. R., Tang, G. Q., Valat, M., & Xie, X. (1998). Prospects of improved oil recovery related to wettability and brine composition. *Journal of Petroleum Science and Engineering*, *20*(3–4), 267–276. https://doi.org/10.1016/S0920-4105(98)00030-8
Nasralla, R. A., Mahani, H., van der Linde, H. A., Marcelis, F. H. M., Masalmeh, S. K., Sergienko, E., et al. (2018). Low salinity waterflooding for a carbonate reservoir: Experimental evaluation and numerical interpretation. *Journal of Petroleum Science and Engineering*, *164*, 640–654. https://doi.org/10.1016/j.petrol.2018.01.028
Nemer, M. N., Rao, P. R., & Schaefer, L. (2021). Coupled influence of wettability alteration and geometry on two-phase flow in porous media. *Advances in Water Resources*, *157*, 104055. https://doi.org/10.1016/J.ADVWATRES.2021.104055
Nicolaides, C., Jha, B., Cueto-Felgueroso, L., & Juanes, R. (2015). Impact of viscous fingering and permeability heterogeneity on fluid mixing in porous media. *Water Resources Research*, *51*(4), 2634–2647. https://doi.org/10.1002/2014WR015811
Ott, H., & Berg, S. (2013). Stability of CO_2-brine primary drainage. *Energy Procedia*, *37*, 4568–4574. https://doi.org/10.1016/j.egypro.2013.06.364
Pau, G. S. H., Bell, J. B., Pruess, K., Almgren, A. S., Lijewski, M. J., & Zhang, K. (2010). High-resolution simulation and characterization of density-driven flow in CO2 storage in saline aquifers. *Advances in Water Resources*, *33*(4), 443–455. https://doi.org/10.1016/J.ADVWATRES.2010.01.009
Peters, E. J., & Flock, D. L. (1981). The onset of instability during two-phase immiscible displacement in porous media. *Society of Petroleum Engineers Journal*, *21*(02), 249–258. https://doi.org/10.2118/8371-PA
Pope, G. A. (1980). The application of fractional flow theory to enhanced oil recovery. *Society of Petroleum Engineers Journal*, *20*(03), 191–205. https://doi.org/10.2118/7660-PA
Rachford, H. H. (1964). Instability in water flooding oil from water -wet porous media containing connate water. *Society of Petroleum Engineers Journal*, *4*(02), 133–148. https://doi.org/10.2118/684-pa
Riaz, A., & Tchelepi, H. A. (2004). Linear stability analysis of immiscible two-phase flow in porous media with capillary dispersion and density variation. *Physics of Fluids*, *16*(12), 4727–4737. https://doi.org/10.1063/1.1812511
Riaz, A., & Tchelepi, H. A. (2006a). Influence of relative permeability on the stability characteristics of immiscible flow in porous media. *Transport in Porous Media*, *64*(3), 315–338. https://doi.org/10.1007/s11242-005-4312-7

Riaz, A., & Tchelepi, H. A. (2006b). Numerical simulation of immiscible two-phase flow in porous media. *Physics of Fluids*, *18*(1), 14104. https://doi.org/10.1063/1.2166388

Saffman, P. G., & Taylor, G. (1958). The penetration of a fluid into a porous medium or Hele-Shaw cell containing a more viscous liquid. *Proceedings of the Royal Society of London, Series A: Mathematical and Physical Sciences*, *245*(1242), 312–329. https://doi.org/10.1098/RSPA.1958.0085

Sall, J., Lehman, A., Stephens, M., & Loring, S. (2012). *JMP start statistics: A guide to statistics and data analysis using JMP*: SAS Institute.

Sarma, H. K. (1986). Viscous fingering: One of the main factors behind poor flood efficiencies in petroleum reservoirs. *Powder Technology*, *48*(1), 39–49. https://doi.org/10.1016/0032-5910(86)80063-8

Schmid, K. S., Geiger, S., & Sorbie, K. S. (2011). Semianalytical solutions for cocurrent and countercurrent imbibition and dispersion of solutes in immiscible two-phase flow. *Water Resources Research*, *47*(2), 2550. https://doi.org/10.1029/2010WR009686

Sorbie, K. S., Al Ghafri, A. Y., Skauge, A., & Mackay, E. J. (2020). On the modelling of immiscible viscous fingering in two-phase flow in porous media. *Transport in Porous Media*, *135*(2), 331–359. https://doi.org/10.1007/s11242-020-01479-w

Sorop, T. G., Masalmeh, S. K., Suijkerbuijk, B. M. J. M., Van Der Linde, H. A., Mahani, H., Brussee, N. J., et al. (2015). Relative permeability measurements to quantify the low salinity flooding effect at field scale. In *Society of Petroleum Engineers - Abu Dhabi International Petroleum Exhibition and Conference, ADIPEC 2015*. Society of Petroleum Engineers. https://doi.org/10.2118/177856-ms

Taheriotaghsara, M., Bonto, M., Eftekhari, A. A., & Nick, H. M. (2020). Prediction of oil breakthrough time in modified salinity water flooding in carbonate cores. *Fuel*, *274*, 117806. https://doi.org/10.1016/j.fuel.2020.117806

Taheriotaghsara, M., Hosseinzadehsadati, S., & Nick, H. M. (2020). The impact of spatially correlated heterogeneity and adsorption on modified salinity water in carbonates. *ACS Omega*, *5*(46), 29780–29794. https://doi.org/10.1021/acsomega.0c03679

Tang, G. Q., & Kovscek, A. R. (2011). High resolution imaging of unstable, forced imbibition in berea sandstone. *Transport in Porous Media*, *86*(2), 617–634. https://doi.org/10.1007/s11242-010-9643-3

Tang, G. Q., & Morrow, N. R. (1997). Salinity, temperature, oil composition, and oil recovery by waterflooding. *SPE Reservoir Engineering*, *12*(04), 269–276. https://doi.org/10.2118/36680-PA

Tchelepi, H. A., & Orr, F. M. (1994). Interaction of viscous fingering, permeability heterogeneity, and gravity segregation in three dimensions. *SPE Reservoir Engineering*, *9*(04), 266–271. https://doi.org/10.2118/25235-PA

Tripathi, I., & Mohanty, K. K. (2008). Instability due to wettability alteration in displacements through porous media. *Chemical Engineering Science*, *63*(21), 5366–5374. https://doi.org/10.1016/j.ces.2008.07.022

Wang, X., & Alvarado, V. (2016). Analysis of capillary pressure and relative permeability hysteresis under low-salinity waterflooding conditions. *Fuel*, *180*, 228–243. https://doi.org/10.1016/j.fuel.2016.04.039

Webb, K. J., Black, C. J. J., & Edmonds, I. J. (2005). Low salinity oil recovery - The role of reservoir condition corefloods. In *13th European symposium on improved oil recovery 2005* (pp. 95–101). European Association of Geoscientists & Engineers. https://doi.org/10.3997/2214-4609-pdb.12.c18

Yortsos, Y. C., & Hickernell, F. J. (1989). Linear stability of immiscible displacement in porous media. *SIAM Journal on Applied Mathematics*, *49*(3), 730–748. https://doi.org/10.1137/0149043

Yuan, Q., Ma, Z., Wang, J., & Zhou, X. (2021). Influences of dead-end pores in porous media on viscous fingering instabilities and cleanup of NAPLs in miscible displacements. *Water Resources Research*, *57*(11), e2021WR030594. https://doi.org/10.1029/2021WR030594